Research Repository UCD

Title	Flight optimization algorithms for aerial LiDAR capture for urban infrastructure model generation
Authors(s)	Hinks, Tommy, Carr, Hamish, Laefer, Debra F.
Publication date	2009-11
Publication information	Hinks, Tommy, Hamish Carr, and Debra F. Laefer. "Flight Optimization Algorithms for Aerial LiDAR Capture for Urban Infrastructure Model Generation." American Society of Civil Engineering (ASCE), November 2009. https://doi.org/10.1061/(ASCE)0887-3801(2009)23:6(330).
Publisher	American Society of Civil Engineering (ASCE)
Item record/more information	http://hdl.handle.net/10197/2294
Publisher's version (DOI)	10.1061/(ASCE)0887-3801(2009)23:6(330)

Downloaded 2026-05-01 23:47:56

The UCD community has made this article openly available. Please share how this access benefits you. Your story matters! (@ucd_oa)

© Some rights reserved. For more information

Flight Optimization Algorithms for Aerial LiDAR Capture for Urban Infrastructure Model Generation

Tommy Hinks[1], Dr. Hamish Carr[2], and Dr. Debra F. Laefer, M.ASCE[3]

Abstract

Aerial Light Detection and Ranging (LiDAR) offers the potential to auto-generate detailed, three-dimensional (3D) models of the built environment in urban settings. Auto-generation is needed as manual generation is not economically feasible for large areas, and yet such models would offer distinct advantages for a wide range of applications from improved noise and pollution prediction to disaster mitigation modeling. Current technology and the dense geometry of urban environments are two major constraints in LiDAR scanning. This paper outlines the difficulties related to effective vertical surface data capture in an urban environment for the purpose of 3D visualization. Further, the traditional point data captured with LiDAR scans is unsuitable for visualization. Therefore, surface reconstruction algorithms must be applied to the data. These algorithms are largely dependent on the uniformity of the resolution in the point data. Principles for geometric optimization of data capture on vertical surfaces, thereby improving resolution uniformity, are presented.

CE Database subject headings: *LiDAR; visualization*; aerial surveys; remote sensing; urban studies; three-dimensional models; geographic information systems.

Introduction

Urban Planners and Civil Engineers require large-scale three-dimensional (3D) geometric models of urban areas for a wide range of applications. These can include such seemingly disparate applications as predictive noise and pollution models or disaster mitigation. In the event of sudden infrastructure changes, such applications require accurate geometric models, and

[1] Doctoral Candidate, School of Computer Science and Informatics, University College Dublin.

[2] Lecturer, School of Computer Science and Informatics, University College Dublin.

[3] Corresponding Author, Director of Conservation Research, School of Architecture, Landscape and Civil Engineering, College of Engineering, University College Dublin, Earlsfort Terrace, Room 113, Dublin 2, Ireland 011-353-1-716-7276 (phone), 011-353-1-716-7399 (fax). Email: debra.laefer@ucd.ie.

in a post-disaster scenario, the models must be acquired rapidly as well. Aerial Light Detection and Ranging (LiDAR) technology holds the potential for rapid auto-generation of such models. This paper discusses the geometric impediments that complicate data capture on vertical building surfaces in urban environments. The discussion is followed by optimizations of the aerial LiDAR flight plan that improve data quality for 3D building modeling purposes.

Background

Increasingly, large-scale computing efforts are being applied to urban planning and disaster management (Laefer and Pradhan 2006; Radke et al. 2000). These range from optimizing single-incident fire department responses to predicting and mitigating regional flooding effects (Kevany 2003; Haile 2005). Many of these efforts have relied upon geographic information systems (GIS). Typically, governmental agencies maintain base maps of their jurisdiction. The majority of these base maps are limited to two-dimensional (2D) representations, with 3D functionalities being limited to a highly narrow set of applications [e.g. to assess the impact of natural disasters (Haile 2005; Veldkamp et al. 2001)]. In coming decades, as population and urbanization expand, threats to quality of life issues (e.g. preservation of natural resources, green spaces, air quality, historic structures, quiet zones) will continue to intensify. As such, better computer modeling capabilities related to these topics will be needed. Visualizing the large data-sets involved in city-scale surveys is challenging (e.g. Popescu et al. 2003). Aerial LiDAR scans generate large collections of points, so called point clouds. These point clouds are unsuitable for visualization and engineering purposes because of their unstructured nature. The task of visualizing LiDAR data can be divided into two areas: (1) reconstructing surfaces (e.g. Zwicker and Gotsman 2004) from point clouds, a noise-sensitive procedure, the success of which is largely dependent on the quality of the sampled points, and (2) visualization of reconstructed surfaces, where efficient scene representations and caching methods must be employed in order to allow modern rendering engines to cope with the enormous data-sets involved. Visualization is crucial to understanding and analyzing large data-sets, and is therefore a critical issue in large-scale urban planning.

Visual System Population

Populating visual GIS systems has been done in a variety of ways. Many of the issues in visual GIS system population are also encountered when populating virtual cities (only some of which are GIS-based). The goal of accurately detailing the built environment requires large data sets. The typical result is a graphically enhanced system that provides 2D images applied to various surfaces within the system. One approach to this is to combine simple 3D models with detailed, real-world texture maps. Jepson and associates did this by overlaying a GIS-based terrain and aerial photographs to position the final models with respect to the road network (Jepson et al. 1996). A sophisticated version of this was used in the Virtual Dublin project which used 3DS Max to model the surface structure of buildings, with digital photographs mapped on top to improve the accuracy of the models (Hamill and O'Sullivan 2003). Other approaches are described below.

Modeling from Imagery

Early attempts at modeling from imagery employed a photogrammetric method to reconstruct scene geometry from photographs. The reconstructed models were then textured in a view-dependent fashion, with the texture manually selected from the original photographs. Texture warping relied upon computed depth information (Debevec et al. 1996). Similarly, in the MIT City Scanning Project extensive research was conducted towards automated data capture for urban simulation (Teller 2005). Façade structure and texture was auto-extracted from calibrated pose imagery (Coorg 1998). This method used sets of images from known positions, which were then correlated to extract the vertical façade features. Wang and associates extended this technique with the recovery of microstructure features, such as recessed windows, by incorporating multiple images of the same structure from different angles (Wang et al. 2002). These techniques rely on calibrated cameras being used from a known global positioning system (GPS) position. Similarly, Lee and associates developed a method for automatically texturing the facades of building models that had previously been generated from aerial photographs by estimating the camera pose data and extracting the texture for the façade automatically from ground-based photographs (Lee et al. 2002).

Modeling from Procedural Generation

Since a visualized city needs to be comprised of strictly site-specific, real-world data, details for a virtual city can be generated using various approaches. By concentrating resources on well-known areas and central landmarks, artificially generated data can be used to complete more distant geographic areas, with sufficient variety and detail without loss of credibility. Parish and Müller employed such an approach using an L-system grammar following topography and population density maps (which may be real or artificially generated) as the basis for the road network generation (Parish and Müller 2001). Their system then divided the blocks between roads into allotments and used another L-system to create building models. The buildings were detailed using combinations of façade textures. Alternatively, a template-based method can be used, which gives more flexibility and variation to the road networks (Sun et al. 2002).

To create a virtual Manhattan, building generation was guided by user input related to building type and supplemented by manual building insertion (Yap et al. 2002). Alternatively, shape grammars can be exploited to generate building models, which allows rapid development of detailed, varying building models, according to rules derived from the real world (Wonka et al. 2003). In contrast, building footprints from GIS Landline map data and aerial LiDAR can be combined to extrude buildings (Laycock and Day 2003).

Virtual City Examples

A sampling of available virtual cities shows a wide variety of end uses and technological orientations, from strictly manual constructions to grammar based modeling, and visual, auditory and haptic response feedback (Dikiaiakou et al. 2003; van Veen et al. 1998). High-end visualization solutions are often developed for the gaming community, which rely on generating plausible facsimiles of urban areas as a part of their gameplay. The modeling of London for the game “The Getaway” (SCEE 2002) was constructed by manual data acquisition and modeling in and the application of acquired textures for facades in a similar fashion to that employed in the Virtual Dublin project (Hamill and O’Sullivan 2003). In all of these cases, what remains a limitation for their transformation into engineering applications is that the information is immutable. Remote sensing holds the potential to overcome this hurdle.

Engineering System Population

Intelligently populating a GIS-based system for high level engineering analysis requires three things: (1) collecting data in a manner that is timely, cost-efficient, and inherently compatible with the existing GIS-based system, (2) obtaining data of sufficient accuracy and detail that the resulting information is meaningful to the end user, and (3) manipulating, coding, and archiving the data in a format from which key parameters can be extracted as input parameters relevant to conduct engineering analyses. Aerial LiDAR may be the most economical solution that suits these three requirements.

LiDAR is an active remote sensing technology that is used to collect topographic data. The data are collected with aircraft-mounted lasers capable of recording distance measurements at a rate of 5,000 to 50,000 pulses per second. The difference in time is measured from when a laser pulse is emitted from a sensor to when the closest object in the path of the laser reflects back the pulse. Using the speed of light, these time measurements can be converted into distance or range. The LiDAR instruments collect range data from known locations as the aircraft moves along the flight path. A high-precision GPS antenna, mounted on the aircraft, is used to determine the spatial positions of aircraft, and so indirectly the positions of the data points collected, since these are offset from the aircraft at given directions and distances. A range data collection can easily be converted into an elevation map by finding the maximum elevation for each point in the ground plane (Baltsavias 1999a). The end product is accurate, geographically registered longitude, latitude, and elevation from the mean sea level (x, y, z) positions for every data point. Latitude, longitude, and elevation are typically presented in a plane co-ordinate system.

LiDAR is capable of providing both horizontal and vertical information at high spatial resolutions and vertical accuracies. In the horizontal plane, airborne-based LiDAR data are accurate to +/- 15 cm for range measurements and +/- 1.5 m (worst case scenario) in the ground plane (Latypov 2003), although systems are sometimes marketed as having higher accuracy than this. The extent of LiDAR point density is dependent on flying height and system related factors, such as platform velocity, sampling frequency, and field of view (Axelsson 1999). The point density needs to be adjusted according to the application so that sufficient information is harvested, while not collecting excessively detailed data. LiDAR technology has been used in

many areas of applications such as (a) generation for a variety of GIS related products, (b) forestry, (c) coastal engineering, (d) flood plain mapping, (e) disaster response and damage assessment, and (f) urban modeling (e.g. Haala 1999; Früh et al. 2005).

An advantage of aerial LiDAR is that it is possible to collect 3D information for thousands of buildings in only a few hours. The data can then be tied directly to a GIS base map. Los Angeles has employed this approach to document its pre-earthquake, baseline condition (Vu et al. 2004). In case of a major earthquake, Los Angeles can be flown immediately again with the LiDAR, and an automated comparison of the images can be conducted. The disaster management community believes that through this approach, unprecedented levels of critical information will be available for decision-making regarding post-earthquake deployment of limited emergency personnel and resources.

Such an approach, however, is restricted currently to a 2D consideration of the community. The buildings models are typically of an extruded or instantiated nature and do not reflect the true geometric and material characteristics of the façades and other vertical faces. Such features are known to be essential in the modeling of a variety of topics including blast-energy dissipation, urban wind tunnels, and pollution modeling (Hu et al. 2004; Mass and Vosselman 1999; Rottensteiner 2003). The current alternative is modeling urban geometry by hand, using modeling software, but this is both slow and inaccurate (Hamill and O'Sullivan 2003; Hamill et al. 2005).

In contrast, although not traditionally employed this way, aerial LiDAR scanning offers the potential to efficiently and rapidly generate accurate geometric models for large urban areas. Traditionally, aerial LiDAR scans have provided high quality data only of horizontal surfaces, as in the case of digital elevation models (e.g. Laefer and Pradhan 2006). Vertical surfaces, however, are harder to capture accurately, principally because the laser beam strikes them obliquely, but also because of shadowing effects. Früh and Zakhor (2003) merge ground scans of vertical surfaces with data collected by aerial LiDAR on horizontal surfaces in an attempt to overcome the problems associated with obliquity in aerial scans. This approach, however, is not always feasible, since the ground-data acquisition is much slower than flying over an area since

it requires traveling along the streets at ground level. Also, in the case of sudden infrastructure changes (e.g. earthquake or blast explosion), acquiring the ground scans may be impossible. However, aerial scans also have limitations, mostly concerning sampling quality on vertical surfaces.

Both obliquity and shadows generate *dead zones* – regions in which data capture is either poor or non-existent. In particular, dead zones are generated by scan obliquity, façade shadows (building self-shadows) and canyon shadows (inter-building shadows). Thus, collecting good quality LiDAR data for vertical surfaces involves planning a flight path to minimize these effects. The remainder of this paper, therefore, analyzes these geometric constraints and provides recommendations on how to plan a suitable flight path to minimize these negative effects for a particular urban environment.

Analyzing Sampling Resolution

Resolution is a measurement of sampling quality. More specifically, resolution in a spatial context is the distance between consecutive samples. Samples in this context are understood to be data points obtained by aerial LiDAR scans. Sampling quality along two principal directions will be discussed in this section. The first is the *along-track* direction, tangent to the flight path. The second is the *across-track* direction, perpendicular to the flight-path.

Contractors carrying out aerial LiDAR scans typically quote the quality of the data obtained in the unit scan points per square meter. For purposes herein outlined, this must first be converted to *linear resolution* (R_L), the resolution in the along-track direction, which is assumed to be constant. Secondly conversion into *horizontal resolution* (R_H), the sample spacing at ground level in the across-track direction is necessary. Finally conversion into *vertical resolution*, the vertical sample spacing on building sides must occur. Of these, the first two will be discussed next. The vertical resolution will be discussed in the section Vertical Scan Obliquity.

Linear Resolution

The figure quoted for scan quality by contractors is notionally the number of scan points per square meter at *nadir* – the point at ground level directly beneath the scanner. For the sake of

argument it is assumed that $R_L = R_N$. This assumption is based on the fact that it is generally desirable to have uniform resolution throughout the entire set of collected scan points. As will be shown further on, this is impossible to achieve in practice because of variations in horizontal and vertical resolution in the across-track direction.

If S is the number of scan points in $1\,m^2$, it follows that the relationship between S and R_L is $R_L = \sqrt{1/S}$, as shown in Figure 1. Consequently the *surface resolution* (R_S) as a measure of the area that each scan point represents in the sampled scene is related to R_L, through the expression $R_S = {R_L}^2$. Details with area coverage smaller than R_S will not be recognizable in the data obtained. For example, if R_S is in the order of m^2 per scan point, objects such as fire hydrants and waste bins will not be recognizable.

The ability to estimate the preflight linear resolution in the across-track direction is crucial to the conclusions presented in this paper. Unlike the along-track resolution which is constant and is determined by the way the platform moves during the scanning process, the samples taken across-track are at uniformly spaced *angles,* not uniformly spaced ground resolution. The following section derives an approximation for horizontal resolution based on flight-path altitude and angular resolution.

Notional Horizontal Resolution

As the LiDAR scanner is flown above a city, the laser beam scans a fairly narrow range of angles beneath the scanner – up to 30° away from the vertical. Angular resolution is constant; as the scanner sweeps along the across-track line (i.e. the difference in angle to the scanner from two consecutive scan points is constant). However, horizontal resolution at ground level is not constant. The distances between consecutive samples on the across-track line increase as the distance from nadir increases. Moving in the across-track direction away from nadir corresponds to increasing an offset angle θ_H from the vertical axis directly beneath the scanner. The distance R_H between two consecutive samples depends on the altitude of the scanner (h), the offset angle from the vertical axis (θ_H), and the angular resolution of the scanner, (θ_L). Figure 2

illustrates the relationships between the parameters mentioned above. Note that the angle θ_L is not shown to scale in the illustrations to improve clarity. The horizontal resolution at nadir (R_N) is trivial to compute: $R_N = h \tan \theta_L$.

The sine law is applied to triangle PRS and then substitute for d. Note that the right triangle PQS allows the substitution $\sin \alpha = \cos(90 - \alpha) = \cos(\theta_H + \theta_L)$:

$$\frac{\sin \alpha}{d} = \frac{\sin \theta_L}{R_H} \text{ or } R_H \sin \alpha = d \sin \theta_L \qquad \text{(eqn 1)}$$

$$R_H \cos(\grave{e}_H + \grave{e}_L) = h \sec \grave{e}_H \sin \grave{e}_L \qquad \text{(eqn 2)}$$

$$R_H = \frac{h \sec \grave{e}_H \sin \grave{e}_L}{\cos(\grave{e}_H + \grave{e}_L)} = \frac{h \sec \grave{e}_H \sin \grave{e}_L}{\cos \grave{e}_H \cos \grave{e}_L - \sin \grave{e}_H \sin \grave{e}_L} \qquad \text{(eqn 3)}$$

For small θ_L the denominator of the right-hand side of Equation 3 is approximately equal to $\cos \theta_H$. Using this approximation Equation 3 can be rewritten as:

$$R_H = h \sin \grave{e}_L \sec^2 \grave{e}_H \qquad \text{(eqn 4)}$$

Since θ_L is small $\cos \theta_L$ is approximately equal to $\tan \theta_L$ resulting in eqn 5:

$$R_H = h \tan \grave{e}_L \sec^2 \grave{e}_H \text{ or } R_H = R_N \sec^2 \grave{e}_L \qquad \text{(eqn 5)}$$

From this, the term $\sec^2 \theta_H$ can be interpreted as a scaling factor applied to the scan point spacing directly beneath the scanner. Let θ_W be the maximum offset angle for a given scanner; hence the largest occurring offset angle is $\theta_H = \theta_W$. For a given height, angular resolution, and scan width, the *effective* horizontal resolution (i.e. the worst case resolution, which occurs when $\theta_H = \theta_W$) can be computed. The expression for effective horizontal linear resolution (R_W) is obtained by inserting the height, angular resolution, and maximum offset into Equation 5:

$$R_W = R_N \sec^2(\grave{e}_W) \qquad \text{(eqn 6)}$$

Modern LiDAR hardware is capable of angular resolutions in the order of 0.01 degrees and maximum offset angles of 30°. Inserting $\theta_W = 30°$ into Equation 6 gives that the effective horizontal resolution is approximately 33% larger than horizontal resolution at nadir (R_N), thereby providing nearly uniform horizontal resolution in the across-track direction.

Finally, the degradation of range accuracy caused by the laser beam widening as it travels away from the scanner is not treated in this paper, for reasons explained below. The widening effectively means that sampling is not done at a single point, but rather over a small area, referred to as the *laser footprint*. This phenomenon has been referred to as *beam divergence* (Deems and Painter 2006). The laser footprint can be approximated by the expression $A_L = h\gamma$, where A_L is the laser footprint, h is the altitude of the scanner, and γ is the beam divergence in radians (Baltsavias 1999b). Modern LiDAR systems have beam divergence angles of about 0.3 to 2 milliradians (Baltsavias 1999a). The relatively low heights used in urban scans, combined with the small beam divergence angles of modern hardware, result in laser footprint areas that are close to singular points. Hence, the beam divergence error is negligible and, therefore, ignored in the following discussions.

Geometric Constraints on Flight Paths

There are six principal constraints on designing a suitable flight plan – urban geometry, flight geometry, vertical scan obliquity, self shadows, street shadows, and lateral scan obliquity. Each of these topics is treated in a separate subsection below, followed by a description of the ideal flight plan resulting from these constraints.

Urban Geometry

Since the constraints on flight planning are principally geometric, characteristic geometry of urban environments must be acknowledged. There are three major factors that need to be considered – building geometry, street geometry, and street layout.

Building geometry describes the shape of individual buildings. For structural and economic reasons, most buildings have vertical walls arranged in rectangular or near-rectangular shapes. While not true for buildings such as circular huts or the Guggenheim Museum, the rectilinear pattern is broadly representative of most large urban aggregations and, as such, can be exploited when scanning. However, urban buildings are often closely spaced, abutting, or employing party walls, making it difficult to distinguish individual buildings – a key feature to individual building extraction.

Street geometry describes the shape of small groups of buildings aligned along a common communication and transportation area. Typically, a street consists of two rows of parallel buildings on opposite sides of an open space. Moreover, building plots along a given street are fairly uniform in size and shape, with the result that barring topographic constraints, large parts of a city tend to have multiple streets parallel to each other. This, combined with the preferred rectilinear shape of buildings, tends to impose a strong geometric structure on the city as a whole, which can also be exploited when scanning (Fig. 3).

Street layout describes the overall geometric structure of the city. While older portions of cities can be very complex, most cities fall into three basic patterns – regular rectangular grids, radial layouts, or topographic structures. However, within radial cities, the infill between the major radial streets tends to be rectangular in nature, as does the infill between topographic boundaries. As such, a reasonable approximation of street layout is that it tends to be locally regular but may be irregular at a larger scale. This localized structure can also be exploited when scanning. For simplicity, the balance of this paper will assume that the city to be scanned is locally a rectangular grid, as shown in Figure 3.

Flight Geometry

While the flight path is notionally controllable, in practice it is easiest to fly in a straight line. Thus, most survey flight paths tend to be a set of straight lines (as opposed to a zigzag or radial pattern). Moreover, for a given altitude of flight, the LiDAR unit scans points on the ground, within a relatively fixed lateral offset (although this is dependent on the altitude of the ground). Since each straight line flown corresponds to a rectangular strip of ground scan, flight planning is

principally a question of choosing the rectangular strips to be scanned in such a way that the overlap covers the desired area. Given straight-line flight paths, this means that the most efficient method is to fly a series of parallel flight paths, whose strips between them cover the entire area with only minimal overlap, as shown in Figure 3. For vertical surfaces, however, further adjustments are necessary to surmount geometric problems.

Vertical Scan Obliquity

The principal geometric difficulty with LiDAR scans of vertical surfaces is that as the LiDAR scanner flies above a city, the laser beam scans a fairly narrow range of angles beneath the scanner – up to 30° away from the vertical. Horizontal linear resolution has previously been shown to be rather uniform in the across-track direction. This is illustrated in the left-hand side of Figure 4.

For vertical surfaces, however, as visible by the dimensions on the right side of Figure 4, the spacing of scan points on vertical surfaces becomes increasingly larger as the vertical surfaces approach nadir. Intuitively, this is reasonable, since a vertical surface directly underneath the scanner will be parallel with the laser beam, which will, therefore, strike the entire surface. In other words, the closer a vertical surface is to nadir, the worse the vertical scan resolution on that surface will be.

Since vertical resolution is worst directly beneath the scanner, guaranteeing scan quality of a particular level requires discarding the data directly beneath the flight path, and for some distance off to the side: paradoxically, this *dead zone* of low quality vertical data is the zone of the *highest* quality horizontal scanning. The *flanks* of the scan, in contrast, have the highest quality vertical scan and lowest quality horizontal data, as shown in Figure 4.

From this observation, it follows that the dead zone from one flight path will have to be scanned in the flank of another flight path. Ignoring overlap, this is most conveniently achieved, if the flank is the same width as the dead zone (or possibly a rational fraction of it). The impact on scan quality of the width of the dead zone is addressed later in the paper, but for now, consider that the dead zone and flanks are of equal width, and that each is 1/3 of the total scan width.

As in the case of linear *horizontal* resolution, approximations for linear *vertical* resolution (R_V) can be derived. Defining a vertical offset angle (θ_V) related to the horizontal offset angle by: $\theta_V = 90 - \theta_H$, as shown in Figure 5, is convenient for notation. The horizontal resolution at a particular offset angle θ_H (eqn 4) can then be related to the *effective* vertical spacing through the expression:

$$R_V = R_H \tan(\theta_V - \theta_L) \text{ or } R_V = R_H \tan(90 - \theta_H - \theta_L) \qquad \text{(eqn 7)}$$

Just as for effective horizontal linear resolution, effective vertical linear resolution is defined for a worst case scenario. Since the vertical offset angle θ_V will be largest at the base of a building side, this is used as a conservative assumption. Note that Equation 7 is only a valid approximation up to $\theta_V = \theta_H = 45°$. At this point horizontal resolution (R_H, eqn 4) starts diverging to infinity faster than $\tan(90 - \theta_H - \theta_L)$ converges to zero. However, since LiDAR hardware is only capable of offset angles up to about 30° model validity is not a problem.

Figure 6 shows how R_H (eqn 5) and R_V (eqn 7) vary with horizontal offset angle (θ_H). The angular resolution θ_L is assumed to be 0.01° and the height used is 300m, based on minimum allowed flyover height in urban regions. Note that an offset angle $\theta_H = 45°$ gives $R_H = R_V$.

Self Shadows

In addition to dead zones caused by vertical scan obliquity, not all vertical surfaces in the scan area will appear on the scan, as a result of *shadows* – since the laser is a form of light, it is blocked by solid objects. Furthermore, as any solid object has a side facing the scanner and a side facing away, the side facing away will be *self shadowed* by the side facing toward the scanner, as shown in Figure 7a. The consequence of this, shown in Figure 7b, is that to acquire *both* sides of a given object, there must be (as a minimum criterion) one scan from the left and one from the right.

Even though each flank provides good quality vertical, data, it only does so for half of the vertical surfaces in the zone. Specifically, the flank to the east of the flight path will only provide

data on west-facing surfaces, and the flank to the west of the flight path will only provide data on east-facing surfaces. Complete scan coverage thus requires that every building be covered from both flanks – one from each of two different flight segments (Fig. 8).

It has been established that the highest quality vertical data is obtained in the flanking strips and that a uniform data quality is desirable. Along-track resolution (R_L) is not subject to geometric constraints and is under the control of contractors. In the section Linear Resolution it was assumed that R_L is chosen to be the same as the horizontal resolution at nadir (R_N) in an attempt at achieving uniform resolution. It would, however, be more efficient to chose R_L to match the vertical resolution (R_V) at the edges of the dead zone (i.e. the worst-case). The rationale behind this is that overall resolution is never better than the worst-case scenario, and achieving better resolution in the along-track direction will not improve overall resolution. Presumably, lowering along-track resolution would lead to faster and cheaper flyover scans.

Street Shadows

While self shadows are the result of a building shadowing itself, scans may also be blocked by the effect of street shadows, in which a building is shadowed by another building on the other side of a street. Geometrically, the effect of these shadows depends on the height of the shadowing building and the distance between the two buildings, as can be seen in Figure 9a. If the distance, w, between the buildings is less than $h \tan\theta$, then the bottom of one building will be shadowed by the adjacent building. Although the building height, h, is immutable, the distance between buildings is measured *perpendicular* to the flight path. If the flight path is parallel to the street, these distances are minimized, as shown by width w_1 in Figure 9b. However, flight paths at an angle to the line of the street will effectively increase the distance between buildings, as shown by diagonal, w_2, in Figure 9b.

Using the assumed perpendicular street grid, the optimal flight angle for avoiding street shadows is a 45° to the street grid. This will maximize w_2 for streets in both directions on, a street grid where streets run in two principal, perpendicular directions.

Unfortunately, flying diagonally to the street pattern compromises the resolution on buildings in the sense that the distance between samples in the street direction, [i.e. the *lateral resolution* (R_{LAT})], increases. Figure 10 illustrates the relationship between linear (along-track) resolution (R_L) and lateral resolution: $R_{LAT} = R_L \sec\varphi$. This dictates that the lateral resolution suffers as the angle φ approaches zero. However, as long as the lateral resolution does not exceed the vertical resolution this does not matter, since the area sampling is dependent on both these distances, and will always be limited by the one that is greater. Hence, it is reasonable to sacrifice lateral resolution in exchange for minimizing street shadows.

Lateral Scan Obliquity

A related problem to vertical obliquity is *lateral obliquity* – the orientation of the vertical surface relative to the laser beam. Since the laser beam is perpendicular to the flight path, this implies that horizontal resolution is best for surfaces parallel to the flight path. Although, at first sight this implies that flight segments should be parallel to the street grid, this would cause each building or group of buildings to have to be scanned from four different directions (as seen in Figure 11a), thereby effectively doubling the cost of the scanning by doubling the flight time.

If, however, by flying *diagonally* to the street grid (as shown in Figure 11b), only two distinct scans are required to capture all four walls, provided that a degradation of scan resolution (i.e. increased horizontal spacing of the scan points) is acceptable. Since the vertical resolution is typically much worse than the horizontal resolution, this is generally acceptable. Provided that the horizontal spacing does not increase beyond the vertical spacing, therefore, the number of scans required to capture reasonable vertical building detail can be halved. Moreover, diagonal flight paths also help minimize the negative impact of street shadows.

Flight Planning

As noted above, the simplest approach is to set the dead zone equal in width to the flanks; for example, for a total scan width of 300m, the dead zone and flanks should each be 100m wide. From Figure 8, setting the distance between the flight paths equal to this width is shown, although a slight reduction may be desirable to achieve some overlap and avoid lacunae in the data. Thus, diagonal flights can be seen to be preferred. As such, the ideal flight path will consist

of a series of parallel lines diagonal to the local street grid, spaced at a distance of 1/3 the total scan width (or possibly a rational fraction of it) from each other, in order to guarantee that each building is correctly scanned on all principal faces with a maximum of scan resolution and a minimum of shadowing (Fig. 12).

Case study: Dublin City Center

An aerial scan of parts of the Dublin city center was made, for which Figure 13 shows the flight path in black overlaid on the street grid. Since the street pattern is not in itself a perfectly regular grid it is impossible to fly in straight lines and at the same time guarantee 45º angles with all the streets. Instead the pattern flown attempts to avoid flying along streets and instead tries to be oriented as close to 45º across as many streets as possible. The data from this survey have yet to be processed and analyzed. The results of such work will be the treated in future publications.

Conclusions

Current aerial LiDAR equipment has the potential to return significant amounts of data related to the vertical details of buildings in urban environments. The successful acquisition of such data is, however, highly dependent on understanding where high quality data is acquired with respect to the flight plan, namely in the flanks, instead of at nadir. Therefore, the flight plan should be designed so that it is set diagonally to the main orientation of the structures of interest. Although both of these aspects are readily achievable within the current state of practice, both are counterintuitive. Traditional practice that has to date focused on the capture of surfaces in the horizontal plane, as opposed to those in the vertical. A detailed analysis of the quality of the expected data for vertical planes and the degradation of the data under a variety of circumstances (e.g. building height, flyover height, and street width) will be the subject of future publications. The principles presented here allow for better visualization results due to the fact that a higher level of detail is present in the data. Surface reconstruction from point data is largely dependent on the uniformity of resolution in the point data. The presented method works toward this by sacrificing lateral resolution in exchange for higher vertical resolution and fewer blind spots in the data, which are major impediments for resolution uniformity. Focusing on vertical façades makes sense in urban visualizations since façades have more diverse appearances than for instance roofs or streets. Digital models of cities are being generated for various reasons all over

the world and the algorithm presented here incurs no extra cost since it is simply a different way of thinking about sampling and is therefore, simple to incorporate into existing flyover programs.

Notation

The following symbols are used in this paper:

A_L : Laser footprint area [m]

h : Height [m]

R_H : Horizontal resolution in across-track direction [m]

R_L : Along-track resolution [m]

R_{LAT} : Lateral resolution [m]

R_S : Surface resolution [m^2/scan point]

R_N : Horizontal resolution at nadir [m]

R_W : Effective horizontal linear resolution [m]

S : Scan point density [scan points/m^2]

θ_H : Horizontal offset angle [degrees]

θ_L : Angular resolution [degrees]

θ_V : Vertical offset angle [degrees]

θ_W : Maximum horizontal offset angle [degrees]

γ : Beam divergence [radians]

References

Axelsson, P. (1999). "Processing of laser scanner data – algorithms and applications." *ISPRS Journal of Photogrammetry and Remote Sensing*, vol. 54, no.2-3, pp. 138-147.

Baltsavias, E.P. (1999a). "Airborne laser scanning: basic relations and formulas." *ISPRS Journal of Photogrammetry and Remote Sensing*, vol. 54, no.2-3, pp. 199-214.

Baltsavias, E.P. (1999b). "Airborne laser scanning: existing systems and firms and other resources." *ISPRS Journal of Photogrammetry and Remote Sensing*, vol. 54, no.2-3, pp. 164-198.

Coorg. S. (1998). "Pose Imagery and Automated Three-Dimensional Modeling of Urban Environments." PhD thesis, MIT.

Debevec, P.E., Taylor, C.J., and Malik, J. (1996). "Modeling and rendering architecture from photographs: A hybrid geometry- and image-based approach." *Proceedings of SIGGRAPH '96*, ACM Press, pp. 11-20.

Deems, J. S. and Painter T. H. (2006). "Lidar measurement of snow depth: Accuracy and error sources." *Proceedings of the 2006 International Snow Science Workshop*, Telluride, CO, pp. 384-391.

Dikiaiakou, M., Efthymiou, A., and Chrysanthou, Y. (2003). "Modeling the walled city of Nicosia." *4th International Symposium on Virtual Reality, Archaeology and Intelligent Cultural Heritage*.

Früh, C., Zakhor, A. (2003), "Constructing 3D City Models by Merging Aerial and Ground Views," *IEEE Computer Graphics and Applications*, vol. 23, no. 6, pp. 52-61.

Früh, C., Jain, S., Zakhor A. (2005). "Data Processing Algorithms for Generating Textured 3D building Façade Meshes from Laser Scans and Camera Images." *International Journal of Computer Vision*, Springer Science, vol. 61, no. 2, pp. 159-184.

Haala, N., and C. Brenner. (1999). "Extraction of Buildings and Trees in Urban Environments." *ISPRS Journal of Photogrammetry and Remote Sensing*, vol. 54, no. 2-3, pp. 130-137.

Haile, A.T. (2005). "Integrating Hydrodynamic Models and High Resolution (DEM) LIDAR for Flood Modelling." Thesis. International Institute for Geo-informational Science and Earth Observation, Enschede, The Netherlands.

Hamill, J., McDonnell, R., Dobbyn, S., and O'Sullivan, C. (2005). "Perceptual Evaluation of Impostor Representations for Virtual Humans and Buildings." *Computer Graphics Forum,* Blackwell Publishing, vol. 24, no. 3, pp. 623-633.

Hamill, J. and O'Sullivan, C. (2003). "Virtual Dublin – A Framework for Real-Time Urban Simulation." *Journal of WSCG*, February 3-7, Plzen, Czech Republic, Science Press, vol. 11, no. 1, pp. 221-225.

Hu, J., You, S., Neumann, U., Park, K.K. (2004). "Building Modeling from LIDAR and Aerial Imagery." *Proceedings of the American Society for Photogrammetry and Remote Sensing Fall Conference*, September, Kansas City.

Jepson, W., Liggett, R., and Friedman, S. (1996). "Virtual modelling of urban environments." *Presence*, vol. 5, no. 1, pp. 83-95.

Kevany, M.J. (2003). "Gis in the world trade center attack - trial by fire." *Computers, environment and urban systems*, vol. 27, no. 6, pp. 571–583.

Laefer, D. and Pradhan, A. (2006). "Evacuation Route Selection Based on Tree-Based Hazards Using LiDAR & GIS." *Journal of Transportation Engineering*, ASCE, vol. 132, no. 4, pp. 312-20.

Latypov D. (2002). "Estimating relative lidar accuracy information from overlapping flight lines." *ISPRS Journal of Photogrammetry and Remote Sensing*, Elsevier Science, vol. 56, pp. 236-245.

Laycock, R.G. and Day, A.M. (2003). "Automatically generating large urban environments based on the footprint data of buildings." *SM'03: Proceedings of the 8th ACM Symposium on solid modelling and applications*, pp. 346-351.

Lee, S.C., Jung, S.K., and Nevatia, R. (2002). "Automatic integration of façade textures into 3D building models with a projective geometry based line clustering." *Computer Graphics Forum*, vol. 21, no. 3, pp. 677-686.

Mass, H. and Vosselman, G. (1999). "Two Algorithms for extracting building models from raw laser altimetry data." *ISPRS J. Photogrammetry and Remote Sensing*, vol. 54, no. 2-3, pp. 153-163.

Parish, Y. and Müller, P. (2001). "Procedural modelling of cities." *Proceedings of SIGGRAPH '01*, pp. 301-308.

Popescu, V., Hoffmann C.S., Kilic, S., Sozen, M., and Meador, S. (2003). "Producing High-Quality Visualizations of Large-Scale Simulations". Purdue University Computer Science Dept. Tech Report 03-011. *IEEE Visualization 2003*, October 19-24, Seattle, Washington, pp. 575-580.

Radke, J., Cova, T., Sheridan, M. F., Troy, A., Mu, L., and Johnson, R. (2000). "Challenges for GIS in Emergency Preparedness and Response," *ESRI White Paper*, < http://www.esri.com/library/whitepapers/pdfs/challenges.pdf> (May 5, 2005).

Rottensteiner, F. (2003). "Automatic Generation of High-Quality Building Models from Lidar Data." *IEEE Computer Graphics and Applications*, vol. 23, no. 6, pp. 42-50.

Sony Computer Entertainment Europe (SCEE). (2002). "The Getaway." London. [video game]

Sun, J., Baciu, G., Yu, X., Green, M. (2002). "Template-based generation of road networks for virtual city modelling." *Proceedings of ACM VRST*, pp. 33-40.

Teller, S. (2005). "MIT city scanning project: fully automated model acquisition in urban areas." *MIT CSAIL*, <http://city.lcs.mit.edu/city.html> (April 26, 2007).

van Veen, H.A., Distler, H.C., Distler, H.K., Braun, S.J., and Bülthoff, H.H. (1998) "Navigating through a virtual city: Using virtual reality technology to study human action and perception." *Future Generation Computer Systems*, vol. 14, no. 3-4, pp. 231-242.

Veldkamp, J.G., Bremmer , C.N., Hack, H.R. G.K., Hendriks, M.A.N., Kronieger, R., Ozmutlu, S, and van Deen, J.K (2001). "Combination of 3D-GIS and FEM modelling of the 2nd Heinenoord Tunnel, the Netherlands". *Abstract to the International Symposium. EngGeoCity – 2001 'Engineering Geological Problems of Urban Areas'*, Ekaterinburg, Russia, 30 July – 2 August 2001, pp. 1-8.

Vu, T.T., Matsuoka, M., and Yamazaki, F. (2004). "Employment of LiDAR for Disaster Assessment." *Second International Workshop on Remote Sensing for Disaster Response*, 7-8 October, Newport Beach, CA.

Wang, X., Totaro, S., Taillandier, F., Hanson, A. and Teller, S. (2002). "Recovering façade texture and microstructure from real-world images." *Proceedings of ISPRS Commission III Symposium on Photogrammetric Computer Vision*, Graz, Austria, September, pp. A381-386.

Wonka, P., Wimmer, M., Sillion, F., and Ribarsky, W. (2003). "Instant architecture." *ACM Transactions on Graphics*, vol. 22, no. 3, pp. 669-677.

Yap, C., Bierman, H., Hertzman, A., Li, C., Meyer, J., Pao, H.K., and Paxia, T. A, (2002). "A Different Manhattan project: Automatic statistical model generation." *Proceedings of SPIE Visualization and Data Analysis*, pp. 259-268.

Zwicker, M. and Gotsman, C. (2004). "Meshing Point Clouds Using Spherical Parameterization." *Proceedings of the 2004 Eurographics Symposium on Point-Based Graphics*, June, Zürich, pp. 173-180.

Acknowledgments

Support for this work was generously provided by Science Foundation Ireland, Grant 05/PICA/I830 GUILD: Generating Urban Infrastructures from LiDAR Data.

List of Figures

Figure 1

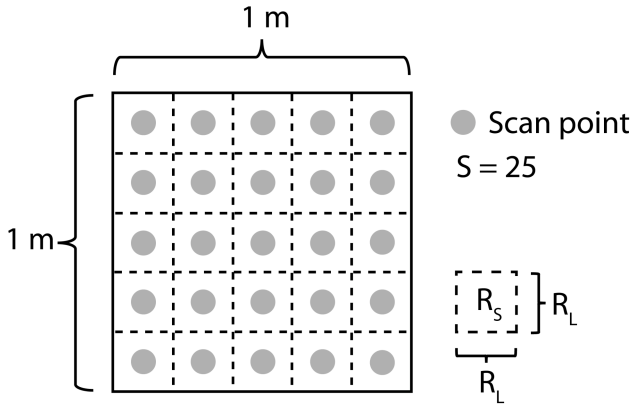

Figure 2

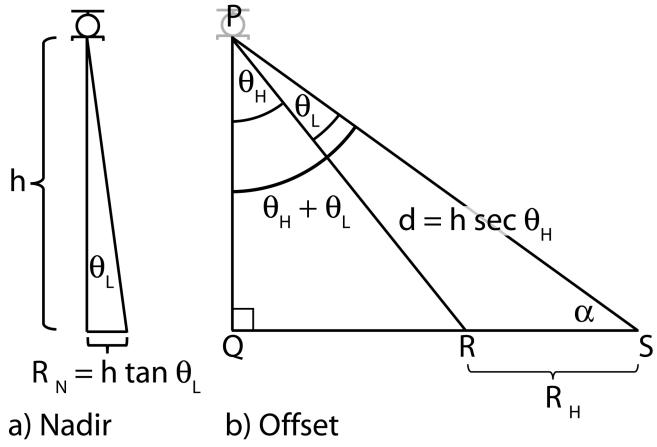

Figure 3

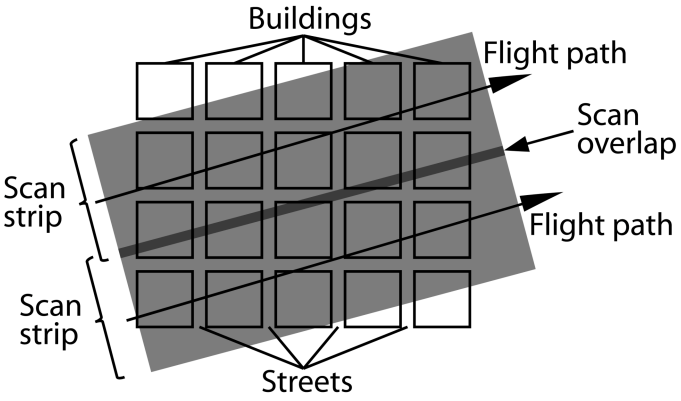
Buildings
Flight path
Scan
overlap
Scan
strip
Flight path
Scan
strip
Streets

Figure 4

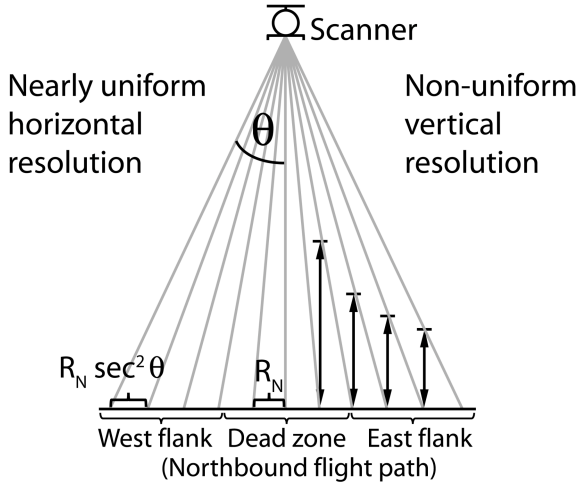
Scanner
Nearly uniform
horizontal
resolution
θ
Non-uniform
vertical
resolution
$R_N \sec^2 \theta$
R_N
West flank
Dead zone
East flank
(Northbound flight path)

Figure 5

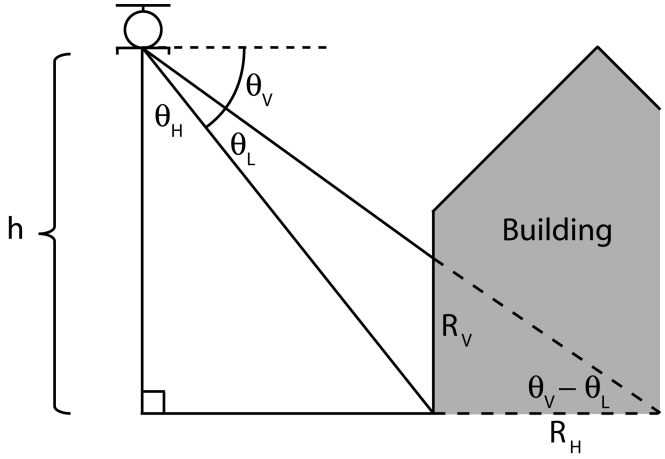

Figure 6

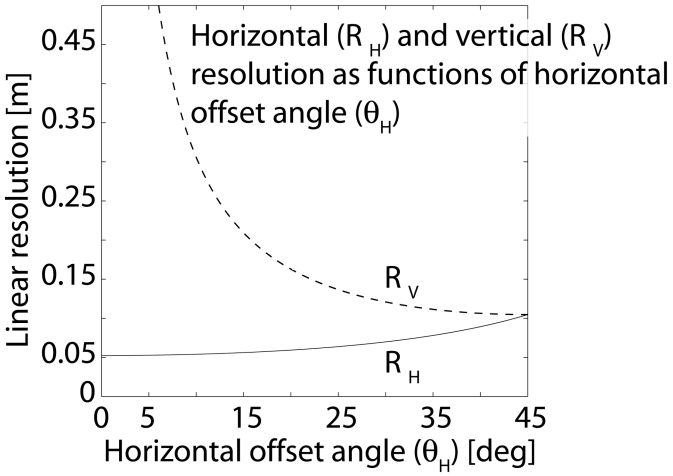
Horizontal (R H) and vertical (R V) resolution as functions of horizontal offset angle (θH)
Linear resolution [m]
0.45
0.35
0.25
0.15
0.05
0
R V
R H
0
5
15
25
35
45
Horizontal offset angle (θH) [deg]

Figure 7

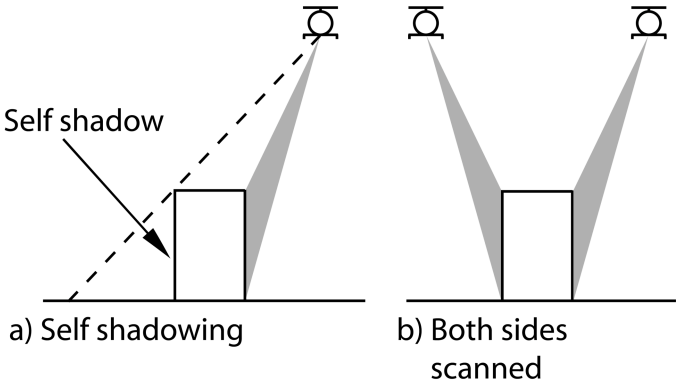

Figure 8

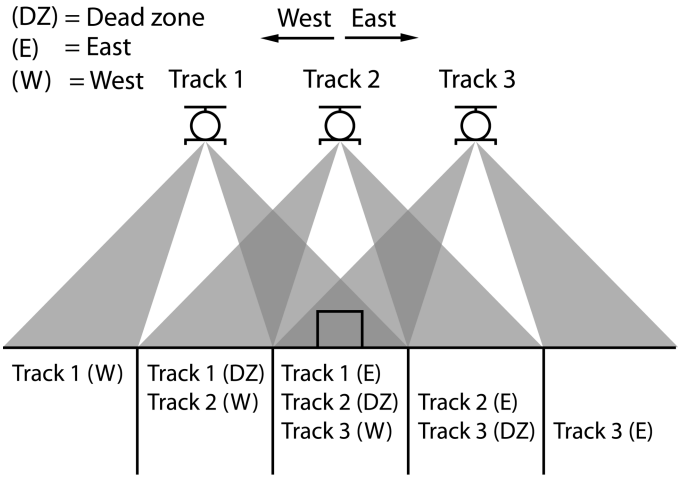
(DZ) = Dead zone
(E) = East
(W) = West
West
East
Track 1
Track 2
Track 3
Track 1 (W)
Track 1 (DZ)
Track 2 (W)
Track 1 (E)
Track 2 (DZ)
Track 3 (W)
Track 2 (E)
Track 3 (DZ)
Track 3 (E)

Figure 9

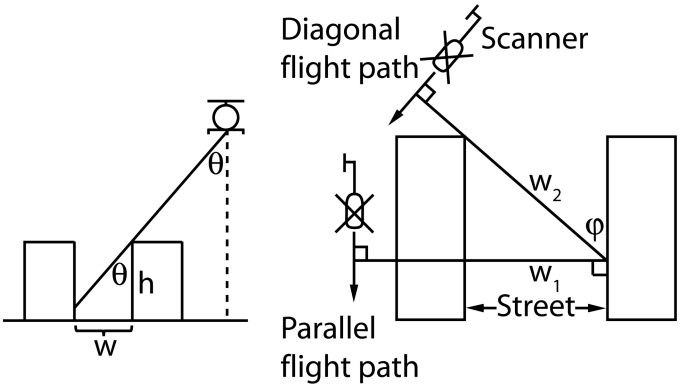

a) Section view b) Plan view

Figure 10

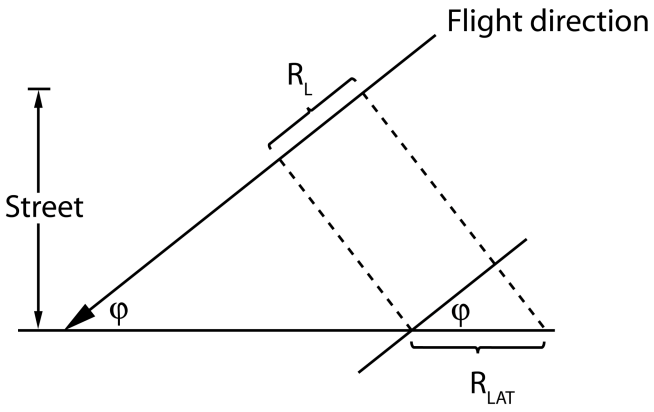

Figure 11

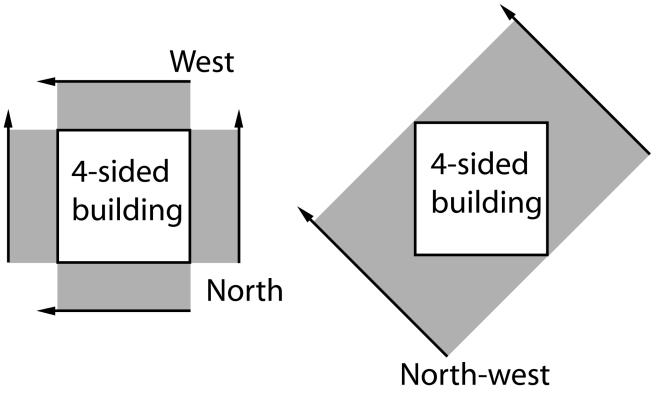

a) Top view b) Top view

Figure 12

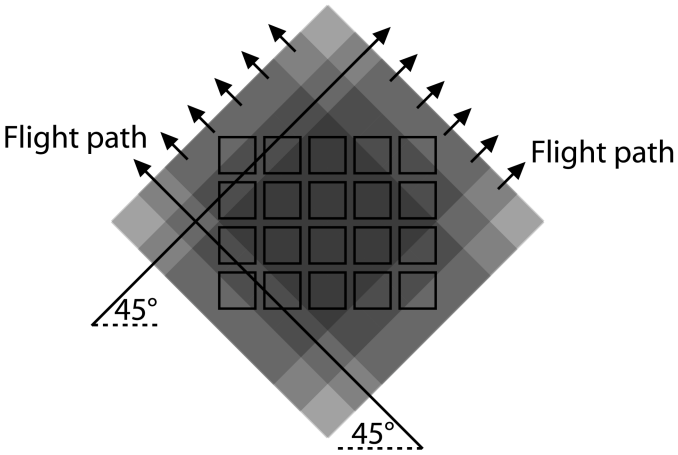

Figure 13